Graphical abstract

TRPM7 kinase is required for insulin production and compensatory islet responses during obesity

Noushafarin Khajavi[1], Andreas Beck[2], Klea Riçku[1], Philipp Beyerle[1], Katharina Jacob[1], Sabrina F. Syamsul[1], Anouar Belkacemi[2], Peter S. Reinach[3], Pascale C F Schreier[1], Houssein Salah[2], Tanja Popp[4], Aaron Novikoff[5, 6], Andreas Breit[1], Vladimir Chubanov[1], Timo D. Müller[5, 6], Susanna Zierler[1, 7], Thomas Gudermann[1, 8]

[1]Walther Straub Institute of Pharmacology and Toxicology, LMU Munich, Germany; [2]Institut für Experimentelle und Klinische Pharmakologie und Toxikologie, Universität des Saarlandes, Homburg, Germany; [3]Wenzhou Medical University, Ophthalmology Department, Wenzhou, P.R. China; [4]Bundeswehr Institute of Radiobiology, Munich, Germany; [5]Institute of Diabetes and Obesity, Helmholtz Center Munich, Neuherberg, Germany; [6]German Center for Diabetes Research (DZD), Neuherberg, Germany; [7]Institute of Pharmacology, Medical Faculty, Johannes Kepler University Linz, Linz, Austria; [8]German Center for Lung Research, Munich, Germany

Corresponding authors:

Prof. Dr. Thomas Gudermann

Walther Straub Institute of Pharmacology and Toxicology Faculty of Medicine, LMU Munich

Goethestr. 33, 80336 Muenchen

Phone: +49 (0)89 2180 75700/2

E-mail: Thomas.Gudermann@lrz.uni-muenchen.de

Dr. Noushafarin Khajavi

Walther Straub Institute of Pharmacology and Toxicology Faculty of Medicine, LMU Munich

Goethestr. 33, 80336 Muenchen

Phone: +49 (0)89 2180 757748

E-mail: Noushafarin.Khajavi@lrz.uni-muenchen.de

Abstract

Most overweight individuals do not develop diabetes due to compensatory islet responses to restore glucose homeostasis. Therefore, regulatory pathways that promote β-cell compensation are potential targets for treatment of diabetes. The melastatin transient receptor potential 7 protein (TRPM7), harboring a cation channel and a serine/threonine kinase, has been implicated in controlling cell growth and proliferation. Here, we report that selective deletion of $Trpm7$ in β-cells disrupts insulin secretion and leads to progressive glucose intolerance. We indicate that the diminished insulinotropic response in β-cell-specific $Trpm7$ knockout mice is caused by decreased insulin production due to an impaired enzymatic activity of this protein. Accordingly, high-fat fed mice with a genetic loss of TRPM7 kinase activity ($Trpm7^{R/R}$) display a marked glucose intolerance accompanied by hyperglycemia. These detrimental glucoregulatory effects are engendered by reduced compensatory β-cell responses due to mitigated protein kinase B (AKT)/ERK signaling. Collectively, our data identify TRPM7 kinase as a novel regulator of insulin synthesis, β-cell dynamics, and glucose homeostasis under obesogenic diet.

Introduction

In obese individuals, a combination of environmental and genetic factors may lead to insulin resistance. The onset of insulin resistance is initially offset by enhanced production and secretion of insulin. However, prolonged demand for elevated levels of circulating insulin may eventually result in β-cell exhaustion, progressive β-cell dysfunction and development of type 2 diabetes (T2D) (1). Identification of signaling molecules which enhance islet compensatory responses in insulin-resistant states may blaze the trail for novel therapeutic approaches to prevent the progression of insulin resistance to T2D.

The transient receptor potential cation channel, subfamily M, member 7 (TRPM7) is a ubiquitously expressed membrane protein, consisting of a divalent cation-selective channel linked to a protein kinase domain. The channel moiety of TRPM7 has been implicated in cellular and systemic Mg^{2+} homeostasis (2, 3). Mg^{2+} plays a key role in maintaining β-cell health, and while Mg^{2+} deficiency impairs insulin secretion and promotes insulin resistance (4), its supplementation improves β-cell function (5). The kinase moiety of TRPM7 belongs to the atypical α-kinase family (6) and has been implicated in controlling numerous cellular processes such as proliferation, growth, migration, apoptosis, differentiation, and exocytosis (7). α-Kinases are structurally and evolutionarily unrelated to conventional eukaryotic protein kinases, yet they share common sequence motifs and the position of key amino acid residues essential for catalysis (8, 9). The remaining dissimilarities of α-kinases to conventional protein kinases are of potential interest for selective pharmacological targeting (10).

In mice, TRPM7 is a central regulator of embryogenesis and organogenesis, with genetic inactivation of TRPM7 causing early embryonic lethality. It has been suggested

81 that localized increases in the concentration of divalent cations due to transmembrane

82 ion flux through the TRPM7 channel trigger kinase activity engaging signaling

83 pathways that are of fundamental relevance in early development (11). There is strong

84 evidence that increases in TRPM7 activity are required to elicit expression of key cell

85 cycle genes in various cell types (12, 13). In hepatic stellate cells, TRPM7 regulates

86 cell proliferation via Phosphoinositide 3-kinases (PI3K) and ERK1/2 signaling

87 pathways (14). In lymphocytes, TRPM7 ablation arrests cell proliferation with a high

88 percentage of arrested cells accumulating at the beginning of the cell cycle, suggesting

89 a potential involvement of TRPM7 in processes orchestrating exit from the

90 quiescence/G0 phase of the cell cycle (15). Notably, TRPM7 inactivation in pancreatic

91 adenocarcinoma cells decreases proliferation and arrests cells in the G0/G1 phases of

92 the cell division cycle (16). The kinase moiety of TRPM7 has been attributed to regulate

93 gene transcription through histone modifications. TRPM7 kinase has been reported to

94 be cleaved from the channel domain in a cell type-specific fashion. It would

95 subsequently translocate to the nucleus and bind to components of chromatin-

96 remodeling complexes (17).

97 Furthermore, TRPM7 plays a role in the regulation of Ca^{2+} signaling in various cell

98 types (18-21). In osteoblasts, the TRPM7 channel modulates cell migration by

99 facilitating Ca^{2+} oscillations (18). TRPM7 has been shown to maintain the Ca^{2+} content

100 of intracellular stores in resting cells. In splenocytes and B lymphocytes, the TRPM7

101 channel and its kinase moieties regulate store-operated Ca^{2+} entry (SOCE) (19, 20).

102 Dysfunctional SOCE in β-cells contributes to the pathogenesis of diabetes and has

103 been reported to disrupt glucose-stimulated Ca^{2+} oscillations in β-cell (22).

104 TRPM7 is highly expressed in human and murine pancreatic β-cells (23, 24). Recent

105 studies revealed that TRPM7 contributes to pancreatic endocrine development and β-

4

106   cell proliferation through modulating intracellular Mg^{2+} levels. Furthermore, it has been

107   suggested that TRPM7 channels augment β-cell glucose-stimulated Ca^{2+} influx in

108   pancreatic β-cells (21). However, it is still not known how changes in TRPM7 kinase-

109   linked activity regulate glucose metabolism and Ca^{2+} signaling in pancreatic β-cells.

110   The present study was designed to clarify the role of TRPM7 in maintaining β-cell

111   function under physiological and metabolically challenged conditions. To decipher the

112   function of TRPM7 in glucose homeostasis, we generated a mouse model with a

113   selective deletion of *Trpm7* in β-cells (β*Trpm7* KO mice*)*. Initially, within 4-weeks (wks)

114   these mice exhibit no overt changes in glucose metabolism following recombination.

115   However, a latent induction of glucose intolerance was evident over 28-wks,

116   suggesting that TRPM7 disruption leads to progressive β-cell dysfunction. In depth

117   metabolic analysis of TRPM7 kinase-dead mice (*Trpm7^{R/R}*) demonstrated that the

118   kinase moiety of TRPM7 is the key player in this scenario. Specifically, our data identify

119   TRPM7 kinase as a crucial cellular component involved in the preservation of

120   glucometabolic islet function under conditions of diet-induced obesity.

121

122

123

124

125

126

Results

Trpm7 deletion in β-cells impairs insulin secretion and glucose metabolism

To assess the requirement of β-cell TRPM7 for insulin secretion and glucose homoeostasis, we generated tamoxifen-inducible β-cell-specific *Trpm7* KO mice (β*Trpm7* KO mice) by crossing *Trpm7flox/flox* with MIP-Cre/ERT mice. Pancreatic islets isolated from β*Trpm7* KO mice reveal efficient β-cell-targeted recombination after tamoxifen-administration. Notably, no Cre-mediated recombination was detected in any region of the brain or liver in β*Trpm7* KO mice (Supplemental Figure 1). We monitored the metabolic phenotype of β*Trpm7* KO mice on regular chow diet within 28-wks. While wild-type and β*Trpm7* KO mice had similar body weight (Figure 1A), the transgenic mice exhibited progressive glucose intolerance starting 16-wks post recombination (Figure 1B-D). Moreover, β*Trpm7* KO mice displayed elevated fed blood glucose relative to control littermates after 28-wks of tamoxifen-induced recombination (Figure 1E). Plasma insulin levels (Figure 1F) and insulin sensitivity (Figure 1G) remained unchanged in both genotypes. Glucose-induced insulin secretion (GIIS) was severely diminished in isolated islets from β*Trpm7* KO mice after 28-wks of tamoxifen-induced recombination. Augmentation of glucose concentrations from 2.8 to 20 mM increased insulin release about 5-fold in wild-type islets, whereas only a 2.5-fold increase of basal insulin exocytosis was observed in the β*Trpm7* KO islets (Figure 1H). Collectively, these data show that tissue-specific TRPM7 disruption in β-cells progressively impairs glucose metabolism, which we hypothesized to be attributable to loss of β-cell identity and impaired cell cycle regulation.

TRPM7 kinase disruption reduces glucose tolerance and glucose-induced insulin secretion

To decipher whether the impaired glucose metabolism is linked to the TRPM7 channel or kinase moiety, we took advantage of a mouse model harboring a single point mutation at the active site of the enzyme ($Trpm7^{R/R}$). We monitored the metabolic phenotype of $Trpm7^{R/R}$ mice within 28-wks. When fed a standard chow diet, $Trpm7^{R/R}$ mice showed no difference in body weight compared to their wild-type controls (Figure 2A, B). However, $Trpm7^{R/R}$ mice displayed glucose intolerance at 8-wks of age that became more prominent in 28-wks old mice (Figure 2C, D, Supplemental Figure 2A). Although the concentrations of blood glucose remained unchanged in fasted and fed 8-wks $Trpm7^{R/R}$ mice relative to controls (Figure 2E), an elevated fed blood glucose was detected in $Trpm7^{R/R}$ mice at 28-wks of age (Figure 2F). Insulin sensitivity and plasma insulin levels remained unaffected within this period (Supplemental Figure 2B-E). This observation pointed to a putative role of the TRPM7 kinase in sustaining islet function and modulating insulin secretion. To test this hypothesis, we investigated GIIS using isolated islets from $Trpm7^{R/R}$ mice and control littermates. In accord with the impaired GTT observed in vivo, TRPM7 kinase disruption reduced maximal insulin secretion capacity in isolated islets (Figure 2G, Supplemental Figure 2F). Augmenting the glucose concentration from 2.8 to 20 mM enhanced insulin exocytosis about 4-fold in wild-type islets, whereas insulin exocytosis only rose 3-fold in isolated islets from 8-wks old $Trpm7^{R/R}$ mice (Figure 2G) and 2.2-fold at 28-wks of age (Supplemental Figure 2F). Membrane depolarization of β-cells by exposure to either 25 mM KCl or 300 μM tolbutamide increased insulin secretion to about 7- and 3.5-fold, respectively, while insulin exocytosis only increased 6.5- and 2-fold in isolated islets of $Trpm7^{R/R}$ mice at

174   8-wks of age. Interestingly, basal insulin secretion was significantly lower in *Trpm7$^{R/R}$*

175   islets relative to wild-type controls (Figure 2G, Supplemental Figure 2F).

176   TRPM7 kinase inactivation has no effect on glucose-induced Ca^{2+}

177   responses and TRPM7 mediated ion currents

178   β-cells display a characteristic Ca^{2+} oscillation pattern in response to high glucose

179   concentration, thus regulating the exocytosis of insulin. Hence, we next asked whether

180   impaired Ca^{2+} responses are attributable to declines in glucose-induced rises in insulin

181   secretion in *Trpm7$^{R/R}$* islets. Exposure to glucose initially induced a rapid increase in

182   [Ca^{2+}]$_i$ followed by continuous oscillations in a subset of wild-type islet cells. *Trpm7$^{R/R}$*

183   islets responded similarly to 20 mM glucose in terms of [Ca^{2+}]$_i$ transients when

184   compared to wild-type islets (Figure 3A, B). The responses to tolbutamide (Figure 3A,

185   C) and KCl (Supplemental Figure 3A, B) under identical conditions were also very

186   similar to one another, confirming that canonical K$_{ATP}$ signaling is not affected by loss

187   of TRPM7 kinase function. Neither the Ca^{2+} oscillation frequency nor the average

188   amplitude of the oscillatory response, were different from one another in both

189   genotypes (Supplemental Figure 4A-C and video 1 and 2). Taken together, these data

190   demonstrate that TRPM7 kinase disruption does not affect glucose-induced Ca^{2+}

191   responses in β-cells.

192   As TRPM7 channels are activated by depletion of intracellular Mg^{2+} (2), we determined

193   the effects of intracellular Mg^{2+} removal on the underlying whole-cell currents in

194   pancreatic islet cells isolated from wild-type and *Trpm7$^{R/R}$* mice (Figure 4A-G). Upon

195   break-in by the patch pipette, most islet cells revealed huge outward currents, probably

196   mediated by a voltage-dependent potassium efflux, which rapidly vanished after

197   infusion of the cesium-based Mg^{2+}-free pipette solution and wash-out of the cytosolic

198   potassium content (Figure 4A). However, within 600 s, small currents with a current-

199   voltage relationship reminiscent of TRPM7 activation developed in both the wild-type

200   (Figure 4B, black trace) and *Trpm7*[R/R] (Figure 4C, purple trace) islet cells. To verify the

201   dependency of these small outward currents on TRPM7 activation, we applied

202   divalent-free external solution (DVF, buffered by EDTA), resulting in significantly

203   increased in- and outward currents in islet cells of both genotypes as a hallmark of

204   TRPM7 activation (Figure 4A-C). Since removal of external divalent cations increases

205   TRPM7`s permeability to monovalent cations, both in- and outward currents increased

206   and the current-voltage relationship switched from slightly outward rectification to a

207   nearly linear shape (Figure 4B and C, blue traces). Figures 4D and E show the current-

208   voltage relations of the basal current-subtracted net TRPM7 current, extracted after

209   600 s (Figure 4D), and the basal current-subtracted net current measured in divalent-

210   free solutions (Figure 4E) in islet cells from wild-type (black traces) and *Trpm7*[R/R] mice

211   (purple). The amplitudes of net TRPM7 currents induced by depletion of free

212   intracellular Mg^{2+} at +80 mV in the presence (Figure 4D, F) and absence of

213   extracellular divalent cations (Figure 4E, G) in islet cells isolated from wild-type and

214   *Trpm7*[R/R] mice were not significantly different, suggesting that in islet cells TRPM7-

215   induced currents are not affected by the presence or absence of its kinase activity.

Genetic loss of TRPM7 kinase does not alter the pancreatic islet cytoarchitecture

218   Next, we asked whether loss of TRPM7 kinase function affects pancreatic islet

219   development. We observed that islet density (Figure 5A, B) as well as islet size

220   distribution (Figure 5C) were similar in both genotypes. Islet size ranged between >45

221   and <420 µm in both genotypes, with the highest frequency found between 61 and

222   180 µm (Figure 5C). In both genotypes, approximately 60 - 70% of the endocrine cells

223   within the islets were insulin-positive β-cells, localized in the central part of the islets,

224 while glucagon-positive α-cells were located at the islet periphery surrounding β-cells

225 (Figure 5A, D). Moreover, the ratio of β- to α-cells remained unchanged in both

226 genotypes (Figure 5E).

227 TRPM7 kinase disruption attenuates insulin biosynthesis

228 Next, we measured the insulin content in islets of both genotypes and noted a

229 remarkable decrease of the insulin content in *Trpm7^{R/R}* islets relative to wild-type

230 controls (Figure 6A). While GIIS was also decreased in *Trpm7^{R/R}* islets (see Figure

231 2G), the GIIS normalized to the content was not significantly different between WT and

232 *Trpm7^{R/R}*. These results indicate that the TRPM7 kinase plays a role in insulin

233 biosynthesis rather than insulin release (Figure 6B). Western blot analysis confirmed

234 the declines in insulin levels (Figure 6C, D). To dissect the cellular mechanism

235 underlying the reduced insulin content of *Trpm7^{R/R}* islets, we performed qRT-PCR

236 analyses and identified reduced expression of key genes involved in insulin production

237 in *Trpm7^{R/R}* islets relative to those in wild-type cells, including: *Ins2*, Pancreatic and

238 Duodenal Homeobox 1 (*Pdx1*) and V-maf musculoaponeurotic fibrosarcoma oncogene

239 homolog A (*MafA*) (Figure 6E). The reduced expression of PDX1 protein in *Trpm7^{R/R}*

240 islets was confirmed by Western blotting and immunohistochemistry (Figure 6F-I). In

241 addition, we demonstrated a remarkable decrease in insulin content as well as

242 expression levels of PDX1 protein in isolated islets from β*Trpm7* KO after 28-wks of

243 tamoxifen-induced recombination (Supplemental Figure 5A-C). These data suggest

244 that the reduced insulin content of *Trpm7^{R/R}* and β*Trpm7* KO islets may be caused by

245 decreased insulin synthesis secondary to a reduction of *Pdx1* expression.

246

247

TRPM7 kinase inactivation impairs HFD-induced β-cell mass expansion

Pdx1 is implicated in compensatory β-cell mass expansion in response to diet-induced insulin resistance (25). Therefore, we examined whether TRPM7 kinase is required for maintenance of pancreatic islet function under HFD feeding. Although cumulative food intake (Figure 7A) was comparable in both genotypes, *Trpm7^{R/R}* mice underwent pronounced increases in body weight and blood glucose levels (Figure 7B, C) and a significant reduction in plasma insulin in the fed state relative to wild-type littermates (Figure 7D). Of note, during HFD feeding, glucose tolerance was severely impaired in *Trpm7^{R/R}* mice relative to wild-type littermates (Figure 7E). Both groups of mice showed similar reductions in blood glucose levels in an insulin tolerance test (Figure 7F). Interestingly, the number of islets per pancreatic section (Figure 8A), as well as the frequency distribution of larger (301-360 μm) islets were reduced, while the distribution of small (0-60 μm) islets was increased in *Trpm7^{R/R}* pancreatic slices (Figure 8B). However, total pancreatic weight did not differ between high-fat fed *Trpm7^{R/R}* and control littermates (Figure 8C). As normal islet compensation involves an expansion of β-cell mass achieved by β-cell hypertrophy and proliferation (26, 27), we examined β-cell size, proliferation, and survival rates in response to HFD. Notably, *Trpm7^{R/R}* islets displayed a significant decrease in β-cell size relative to control littermates (Figure 8D). Ki67 was used as a proliferation marker. The abundance of Ki67-positive β-cells was markedly reduced in *Trpm7^{R/R}* islets compared to control littermates (Figure 8E, F). Thus, these results suggest that loss of TRPM7 kinase restrains β-cell proliferation in response to HFD. Importantly, we did not detect any TUNEL-positive, i.e. apoptotic β-cells in wild-type and *Trpm7^{R/R}* islets (Supplemental Figure 6A). Furthermore, to investigate whether reduced β-cell proliferation in *Trpm7^{R/R}* mice is associated with impaired store-operated Ca^{2+} entry (SOCE), we monitored passive Ca^{2+}-release in

273 response to the sarcoplasmic/endoplasmic reticulum calcium ATPase (SERCA) pump

274 blocker cyclopiazonic acid (CPA) followed by SOCE after Ca^{2+}-re-addition. However,

275 there was no significant difference both in passive Ca^{2+}-release and subsequent SOCE

276 between β-cells derived from $Trpm7^{R/R}$ and wild-type genotypes (Supplemental Figure

277 6B-D).

278 **TRPM7 kinase inactivation reduces expression levels of genes involved in**

279 **insulin production and cell cycle regulation**

280 We investigated the gene expression profile by RNA-sequencing using RNA prepared

281 from isolated islets of high-fat fed $Trpm7^{R/R}$ and wild-type mice. We identified

282 upregulation of 382 genes and downregulation of 1615 genes in $Trpm7^{R/R}$ islets.

283 Interestingly, genes critical to insulin production were found to be down-regulated,

284 including *Ins2*, *Mafa*, *Pdx1*, *Cpe* and *Nkx6-1*. We also observed down-modulation of

285 genes involved in cell cycle regulation, such as cyclin-dependent kinase 4 (*Cdk4*), and

286 *Ccnd2*, and several proliferation markers including *Cirp*, *Mll5* and *Pimerg*

287 (Supplemental Table 1). No changes were observed in the expression levels of genes

288 involved in glucose sensing and exocytosis (Supplemental Table 2). Volcano plot

289 (Figure 8G) and heat maps (Supplemental Figure 7A, B) illustrate the differential

290 expression of genes involved in insulin biosynthesis, cell cycle progression, and

291 cellular proliferation. A summary of the genes involved in insulin production and cell

292 cycle regulation that were down-regulated in islets lacking TRPM7 kinase is shown in

293 Supplemental Figure 7C, D.

294 **TRPM7 Regulates β-cell function via protein kinase B (Akt) and Erk1/2 Signaling**

295 **Pathways**

296 TRPM7 kinase regulates TGFβ/SMAD signaling (28). This signaling pathway has been

297 implicated in various cellular processes including proliferation, differentiation,

12

298 apoptosis, and cell migration (29). To gain insight into the connection between TRPM7

299 kinase and signaling cascades triggering compensatory islet responses to a HFD, we

300 employed a bead-based Bio-Plex assay to simultaneously measure the

301 phosphorylation status of multiple TGFβ/SMAD signaling proteins in the same sample.

302 We examined the phosphorylation status of SMAD2 (Ser465/Ser467), SMAD3

303 (Ser423/Ser425), AKT (Ser473), ERK1/2 (Thr185/Tyr187) as well as total protein

304 levels of SMAD4 in isolated islets from *Trpm7*[R/R] and wild-type mice on a HFD for 16-

305 wks. A slight decrease was detected in the phosphorylation levels of SMAD2 and total

306 SMAD4. However, the differences did not reach statistical significance. *Trpm7*[R/R] mice

307 displayed a significant reduction of ERK-dependent signaling under HFD feeding.

308 Interestingly, our results demonstrated a 40% reduction of AKT phosphorylation in

309 *Trpm7*[R/R] mice fed with a HFD (Figure 8H). Quantification of SMAD3 phosphorylation

310 status was below the detection limit in both genotypes and excluded from the study.

311 Next, we asked whether reduced ERK1/2 and AKT phosphorylation in *Trpm7*[R/R] islets

312 is attributable to the dysfunctional TRPM7 in β-cells. To address this question, we

313 measured the phosphorylation status of ERK1/2 and AKT in isolated islets from

314 β*Trpm7* KO mice and control littermates on 16-wks of a HFD. Notably, β*Trpm7* KO

315 mice demonstrated a significant decrease in both ERK- and AKT-dependent signaling

316 (Supplemental Figure 8A, B), confirming the role of TRPM7 in modulating these

317 signaling cascades in β-cells.

318 **TRPM7 overexpression induces GIIS in MIN6 cells**

319 To test whether enhanced expression of *Trpm7* in β-cells induces insulin secretion, we

320 used cultured MIN6 mouse insulinoma cells as an in vitro model. We transiently

321 transfected MIN6 cells with *Trpm7* WT, *Trpm7*[R/R] plasmids or with empty vector

322 (Supplemental Figure 9A). The MIN6 cells treated with the *Trpm7*[R/R] plasmid had a

323   GIIS response similar in magnitude to that of MIN6 cells treated with an empty vector.

324   In contrast, MIN6 cells transfected with the *Trpm7* WT plasmid displayed a pronounced

325   increase in GIIS (Supplemental Figure 9B). This response pattern is in good agreement

326   with the data obtained with isolated islets from β*Trpm7* KO and *Trpm7*[R/R] mice. Next,

327   we investigated the effect of *Trpm7* overexpression in MIN6 cells on the expression

328   levels of key signaling proteins. Western blotting studies showed that treatment of

329   MIN6 cells with *Trpm7* WT plasmid led to a significant increase in phosphorylated

330   forms of ERK1/2 and AKT (Ser473), as compared to cells treated with empty vectors.

331   The expression levels of total ERK and AKT remained essentially unchanged after

332   *Trpm7* WT overexpression (Supplemental Figure 9C-E).

333

334

335

336

337

338

339

340

341

342

Discussion

We report in here that TRPM7 regulates glucose homeostasis and compensatory pancreatic islet responses via its kinase moiety. Impaired glucose tolerance and glucose-induced insulin secretion were comparable among β*Trpm7* KO and *Trpm7*$^{R/R}$ genotypes. Importantly, mice from both genotypes developed age-dependent rises in dysfunctional glucose metabolism and declines in glucose-induced insulin secretion. Reduced insulin secretion in response to various insulin secretagogues in *Trpm7*$^{R/R}$ suggests a salient role of this α-kinase in maintaining β-cell function. Intracellular Ca^{2+} transients are the final trigger for insulin exocytosis. Studies with *Trpm7*$^{R/R}$ pancreatic islets showed that glucose and high potassium (KCl)-induced Ca^{2+} responses remain unaffected, suggesting that the reduction of glucose-induced insulin secretion in *Trpm7*$^{R/R}$ mice is not caused by impaired Ca^{2+} signaling in β-cells. In addition, TRPM7-like currents in *Trpm7*$^{R/R}$ islets were comparable to those of wild-type cells, demonstrating that the channel moiety of TRPM7 remains intact in this mouse model. Interestingly, we found a pronounced reduction of insulin content accompanied by reduced *Pdx1* transcript and protein levels in *Trpm7*$^{R/R}$ and β*Trpm7* KO mice. In humans, mutations of *Pdx1* are strongly associated with diabetes (30). Previous studies have demonstrated a correlation between low PDX1 levels and β-cell dysfunction (31, 32), because PDX1 directly regulates the expression of the insulin gene and other components of the GIIS pathway including *MafA* (33, 34). Therefore, we suggest that *Pdx1* downregulation might suppress insulin production in *Trpm7*$^{R/R}$ and β*Trpm7* KO mice.

Importantly, *Pdx1* and *MafA* are the key β-cell markers and major transcription factors to maintain β-cell identity. Altered identity of β-cells has been proposed as an underlying mechanism of diabetes progression in patients (35, 36). Furthermore,

368 previous studies linked overexpression of PDX1 to the upregulation of several cell

369 cycle genes and increases in β-cell proliferation (37, 38). Therefore, we attribute the

370 age-dependent progressive impairment in glucose metabolism in $Trpm7^{R/R}$ and

371 β$Trpm7$ KO mice to the gradual loss of β-cell identity and reduced β-cell proliferation

372 due to $Pdx1$ downregulation.

373 Accumulating evidence has underscored the pivotal role of PDX1 in β-cell expansion

374 and survival in response to a HFD challenge (25). Therefore, we set out to define the

375 role of TRPM7 kinase in β-cell survival and compensatory hypertrophy in response to

376 a HFD. Thus, an obesogenic diet resulted in increased body weight, hyperglycemia,

377 reduced insulin levels, and glucose intolerance in $Trpm7^{R/R}$ mice relative to wild-type

378 controls. These phenotypic changes were not caused by severe insulin resistance in

379 $Trpm7^{R/R}$ mice, because insulin tolerance was comparable in both genotypes. It is

380 worth mentioning that high-fat fed $Trpm7^{R/R}$ mice became more severely

381 hyperglycemic than control littermates after 16-wks of obesogenic diet, especially in

382 the fed state. Collectively, our data are compatible with the notion that the pronounced

383 impairment of glucose homeostasis in $Trpm7^{R/R}$ mice is attributable to impaired

384 compensatory β-cell mass expansion and proliferation in response to obesogenic diet.

385 Glucose intolerance observed in the $Trpm7^{R/R}$ mice on the HFD is consistent with the

386 metabolic phenotype of $Pdx1^{+/-}$ animals (39). Like our findings in $Trpm7^{R/R}$ mice, high-

387 fat feeding induced a similar weight gain in $Pdx1^{+/-}$ animals relative to wild-type controls

388 (25). Taken together, we suggest that reduced $Pdx1$ expression in $Trpm7^{R/R}$ mice

389 dampens both insulin production and compensatory β-cell mass expansion, entailing

390 compromised glucose tolerance in high-fat fed $Trpm7^{R/R}$ mice.

391 Prior to our work, Altman $et\ al.$ (2021) observed that β-cell proliferation induced by 2-

392 wks HFD was significantly reduced in TRPM7 deficient β-cells. In agreement with our

393 finding, TRPM7 disruption in β-cells did not alter glucose tolerance within 4-wks of

394 recombination. However, they suggested that reduced proliferation observed after

395 exposure to obesogenic diet is mediated by impeded Mg^{2+} influx into β-cells during

396 proliferation (21). In this context, it is worth mentioning that TRPM7 channel and kinase

397 activities are mutually interdependent, in that the kinase functionality requires the influx

398 of Mg^{2+} through the channel pore (40). Therefore, we put forward an alternative

399 explanation and suggest that hampered β-cell proliferation may be attributable to

400 reduced kinase activity that result from declines in Mg^{2+} levels. Furthermore, our

401 histological studies of $Trpm7^{R/R}$ mice pancreas do not agree with the developmental

402 changes shown by Altman *et al.* (2021) after TRPM7 inactivation (21). This difference

403 might point to the role of the channel moiety of TRPM7 in early events influencing

404 pancreatic endocrine development.

405 RNA-seq studies with RNA isolated from high-fat fed $Trpm7^{R/R}$ and control islets

406 demonstrated that TRPM7 kinase deficiency downregulated the genes involved in

407 insulin biosynthesis, cell cycle progression, and proliferation. Notably, TRPM7 kinase

408 disruption engenders reduced expression of two early G1/S phase molecules, cyclin

409 D2 and *Cdk4* in high-fat fed mice. It has previously been demonstrated that mice

410 lacking *Cdk4* exhibit islet deformity and a reduced size of islets accompanied with

411 diminished insulin production, whereas activation of the CDK4 pathway resulted in β-

412 cell hyperplasia (41). Interestingly, reduced pancreas size in *Cdk4*-deficient mice is

413 thought to result from impaired mesenchymal development and decreased numbers of

414 PDX1^{+} pancreatic progenitor cells (42). Moreover, CDK4 enhances β-cell replication

415 within adult islets and activates progenitor cells within adult pancreatic ductal

416 epithelium in response to partial pancreatectomy (43). We suggest that reduced islet

417 size, and impaired β-cell proliferation in high-fat fed $Trpm7^{R/R}$ mice might at least

418   partially be attributable to reduced CDK4 expression in pancreatic islets. In addition,

419   we noted that the transcript levels of several other proliferation markers including *Cirp*,

420   *Mll5* and *Pimerg* were significantly reduced in high-fat fed TRPM7 *Trpm7^{R/R}* mice.

421   Interestingly, CIRP activation occurs downstream of various stress stimuli and is

422   known to regulate cell survival and cell proliferation, particularly during stress (44).

423   In mouse models of diet-induced obesity, high-fat feeding has been linked to ER stress

424   in β-cells resulting in the inability to trigger an appropriate unfolded protein response

425   (UPR), potentially leading to β-cell apoptosis (45). Previous studies show that *Pdx1^{+/-}*

426   β-cells are more susceptible to ER stress under high-fat feeding (25). PDX1 plays a

427   crucial role in the regulation of genes involved in ER function, including disulfide bond

428   formation, protein folding, and the unfolded protein response. Here, we show the

429   downregulation of several ER-related genes in *Trpm7^{R/R}* islets including genes

430   encoding enzymes critical for disulfide bond formation in the ER (*Pdia4*, and *Pdia6*),

431   ER chaperone (*Hspa5*), and mediators of UPR pathways (*Atf4*), which are direct

432   transcriptional targets of PDX1 (25). Although it has been suggested that *Pdx1*

433   deficiency promotes ER stress-associated cell death, we did not detect apoptosis in

434   wild-type and *Trpm7^{R/R}* islets, even when challenged by high-fat feeding. This

435   observation is fully in line with a recent study by Barrela *et al.* (2021) who did not detect

436   any apoptotic β-cells in β-*barr1*-KO mice in the presence of severely impaired *Pdx1*

437   expression (46). Furthermore, Altman *et al.* (2021) reported that TRPM7 KO has no

438   effect on β-cell apoptosis (21). Previous studies demonstrated that knockdown of *Pdx1*

439   in rat insulinoma cells (INS-1) results in a reduced sarco-endoplasmic reticulum Ca^{2+}

440   ATPase 2b (SERCA2b) expression and decreased ER Ca^{2+} levels (47). Importantly,

441   TRPM7 kinase deficiency has been shown to suppress SOCE in T-cells and B

442   lymphocytes (19, 20). Nevertheless, we found that both SOCE and ER Ca^{2+} storage

443   are unaffected in *Trpm7$^{R/R}$* islets (Suppl. Fig. 6 B, C), ruling out a major impediment of

444   this pathway in pancreatic β-cells from *Trpm7$^{R/R}$* mice.

445   Phosphorylation of PDX1 is required for its nuclear translocation and binding to target

446   promoters (48). PDX1 phosphorylation occurs in response to PI3K/AKT signaling (49)

447   and ERK1/2 (50). Blocking the PI3K/AKT pathway in pancreatic β-cells reduces insulin

448   content and insulin secretion (51). Overexpressing *Akt1* in pancreatic β-cells increases

449   β-cell mass, proliferation and cell size which leads to improved glucose tolerance and

450   insulin secretion (52, 53). A recent study reported that the improvements in glucose

451   tolerance, β-cell proliferation, and β-cell mass induced by enhanced AKT signaling was

452   blunted in PDX1 deficient mice (49). Furthermore, FOXO1 is an established upstream

453   regulator of PDX1. FOXO1 acts as a repressor of FOXA2, which is known to activate

454   the *Pdx1* promoter. Haploinsufficiency of FOXO1 reverses β-cell failure in *Irs2$^{-/-}$* mice

455   through partial restoration of β-cell proliferation and increased expression of *Pdx1* (54).

456   In pancreatic cancer cells, inhibition of PI3K/AKT and MAPK/ERK pathways activates

457   FOXO transcription factors leading to cell cycle arrest and apoptosis (55). Moreover,

458   in pancreatic β-cells, mitogen-activated protein kinases ERK1/2 have been shown to

459   be the major expressed forms of ERKs, playing an essential role in mediating cell

460   proliferation (56, 57). TRPM7 is a known regulator of the PI3K/AKT, SMAD, and

461   ERK1/2 signaling pathways (29, 58). Our data suggest that TRPM7 kinase might

462   directly or indirectly phosphorylate AKT and ERK1/2. Activation of the AKT and ERK1/2

463   pathways enhances PDX1 transcriptional activity, leading to compensatory β-cell

464   hypertrophy and proliferation. However, it is worth mentioning that AKT also induces

465   proliferation of β-cells through direct regulation of cyclin D1, cyclin D2, and CDK4 levels

466   (59). Our results do not exclude the possibility that TRPM7 kinase might be involved in

467   β-cell cycle regulation and proliferation in a PDX1-independent manner. To further

corroborate the concept that TRPM7 kinase regulates AKT/ERK signaling, we transfected MIN6 cells with *Trpm7* WT, *Trpm7$^{R/R}$*. We found that overexpression of *Trpm7* WT in MIN6 cells enhances phosphorylation of ERK1/2 and AKT and leads to increases in insulin secretion. These results further support the notion that the detrimental glucoregulatory effects in *Trpm7$^{R/R}$* mice are due to mitigated AKT/ERK signaling.

Obesity is a leading pathogenic factor for developing insulin resistance. Insulin resistance in obese individuals triggers a compensatory response in pancreatic islets. In this study, we provide evidence that TRPM7 kinase regulates insulin production and elicits an appropriate compensatory islet response to an obesogenic diet. Furthermore, the results from this study point to a potential link between TRPM7 kinase activity and the expression of critical genes required for insulin biosynthesis and cell cycle regulation. Therefore, we identify TRPM7 kinase as a critical cellular gatekeeper to preserve and improve β-cell function under metabolically challenging circumstances.

Material and methods

489

490 ***Mouse strains and genotyping procedures.*** MIP-Cre/ERT and *Trpm7^{tm1Clph}*

491 *(Trpm7^{flox/flox})* mice were obtained from Jackson Laboratory. *Trpm7tm1.1Mkma*

492 *C56BL/6* (K1646R, *Trpm7^{R/R}*) mice were kindly provided by Prof. Masayuki Matsushita

493 (Okayama University Medical School, Okayama, Japan). *Trpm7^{flox/flox}* mice (60) and

494 *Trpm7^{R/R}* mice (61) were reported previously. Mice were backcrossed to C57BL/6 (≥ 6

495 generations). Mice were housed in ventilated cages at the animal facility of the Walther

496 Straub Institute of Pharmacology and Toxicology, LMU, Munich, Germany. *Trpm7^{flox/flox}*

497 and MIP-Cre/ERT mice were bred to obtain age- and gender-matched homozygous

498 *Trpm7^{flox/flox}*;MIP-Cre/ERT mice. To induce Cre activity in β-cells of adult mice, 8-week-

499 old male *Trpm7^{flox/flox}*;MIP-Cre/ERT mice were injected i.p. with tamoxifen in corn oil

500 (2 mg/day/mouse for 5 consecutive days). Negative controls were *Trpm7^{flox/flox}*;MIP1-

501 CreERT mice, which received just injections of corn oil. Heterozygous K1646R animals

502 were bred to obtain age- and gender-matched homozygous wild-type and homozygous

503 *Trpm7^{R/R}* mice. For genotyping, DNA was extracted from ear fragments using the

504 Mouse Direct PCR Kit (Biotool). DNA samples were analyzed by PCR using a set of

505 allele-specific oligonucleotides (Metabion). Sequence information is provided in

506 Supplemental Table 2. Genotyping of *Trpm7^{flox/flox}* and *Trpm7^{R/R}* mice were performed

507 as previously described (3). Inheritance of MIP-Cre/ERT transgene was determined by

508 PCR using the following condition: 94 °C 2', 94 °C 15'', 60 °C 15'', 72 °C 10'', 30 cycles.

509 Male and female mice were fed chow diet or diabetogenic diet (Research Diets,

510 D12451), containing 45% kcal from fat, beginning at 8-wks of age. Mice were single-

511 or group-housed on a 12 h/12 h light-dark cycle at 22 °C with free access to food and

512 water. Mice were maintained under these conditions for a maximum of 36-wks.

Characterization of Glucose Homeostasis. For the determination of glucose tolerance, 8- or 24-week-old mice (male and female) were fasted overnight (16 hours). Basal blood glucose was sampled, and glucose was administered as an intraperitoneal (i.p.) injection at a dose of 2 g/kg body weight (20% w/v D-glucose (Sigma) in 0.9% w/v saline). Blood samples were obtained from the tail vein. Blood glucose levels were measured by glucometer (TheraSense FreeStyle) before (0 min) and at 15, 30, 60, and 120 min after injection. For the determination of insulin tolerance, mice were fasted for 4 hours at the onset of the light cycle and injected intraperitoneally with 0.75 units of insulin per kg body weight. Blood glucose levels were measured by glucometer (TheraSense FreeStyle) before (0 min) and at 15, 30, 60, and 120 min after injection. For investigation of blood parameters, blood was collected after euthanasia using EDTA-coated microvette tubes (Sarstedt), immediately cooled on ice, centrifuged at 2,000 × g and 4 °C for 10 min, and plasma stored at −80 °C. Plasma insulin was quantified by an Insulin ELISA assay (ALPCO, Salem, US).

Islet Isolation and Determination of Insulin Secretion. Islets were isolated from 8- to 36-wks-old male and female mice. Isolation of pancreatic islets was performed as previously described (62). In brief, pancreas was perfused by injection of 3 mM Collagenase-P (Roche, Mannheim, Germany) (0.3 mg/ml) in Hank's buffered salt solution (HBSS) containing 25 mM HEPES and 0.5% (w/v) BSA into the common bile duct. Isolated islets were recovered for 48 hours in RPMI 1640 (Thermo Fisher Scientific, Germany) in humidified 5% CO_2, at 37 °C. After this period, islets were used for functional assessments. Before determination of insulin secretion, islets were equilibrated for 1 hour in KRB-Buffer (115 mM NaCl, 4.5 mM KCl, 1.2 mM KH_2PO_4, 2.6 mM $CaCl_2$, 1 mM $MgCl_2$, 10 mM HEPES, 20 mM $NaHCO_3$, 0.2% (w/v) BSA, pH 7.4) with 2.8 mM glucose. Determination of insulin secretion from the islets was

performed in 12-well plates containing 60 µl KRB (8 islets/well, 5 independent experiments performed in triplicate). After 1 hour preincubation in KRB with 2.8 mM glucose, islets were incubated for 1 hour in 20 mM glucose, 25 mM KCl or 300 µM tolbutamide. Released insulin was measured in the supernatant using an insulin ELISA kit (ALPCO, Salem, US). Insulin content was determined from groups of ten islets lysed in the protein extraction reagent M-PER (Thermo Fisher Scientific), using insulin ELISA kit.

Calcium Imaging. Islets were loaded with 4 µM fluo-4 AM (Invitrogen) for 2 hours at room temperature in extracellular buffer containing 138 mM NaCl, 5.6 mM KCl, 2.6 mM CaCl$_2$, 1 mM MgCl$_2$, and 5 mM HEPES, pH 7.4. Changes in $[Ca^{2+}]_i$ were recorded by laser scanning confocal microscopy using an LSM 510 Meta system (Zeiss) using a water immersion objective (63X/NA1.2). Individual cells were selected as "regions of interest" with the LSM software, and their calcium responses to the different stimuli were measured as alterations in fluo-4 emission intensity at 500–550 nm upon excitation with the 488 nm line of an argon laser. 8-bit 512×512 pixels images were acquired every 5 s. Calculation of calcium oscillation frequency and amplitude is described in detail in supplementary information.

Electrophysiological Recordings. Whole cell membrane currents were recorded using an EPC-9 amplifier (HEKA Electronics, Lambrecht, Germany). Patch pipettes were pulled from glass capillaries GB150T-8P (Science Products, Hofheim, Germany) at a vertical Puller (PC-10, Narishige, Tokyo, Japan) and had resistances of 3 to 4 MΩ when filled with internal solution. The internal solution (0 Mg) comprised of (in mM) 120 Cs-glutamate, 8 NaCl, 10 HEPES and 10 Cs-EDTA to chelate internal divalents (pH adjusted to 7.2 with CsOH). The extracellular solution contained (in mM) 140 NaCl, 2 MgCl$_2$, 1 CaCl$_2$, 10 HEPES, 10 glucose (pH adjusted to 7.2 with NaOH). Divalent-free

563 solution (DVF; $CaCl_2$ and $MgCl_2$ were omitted from the external solution and 5 mM Na-

564 EDTA was added) was directly applied onto the patch-clamped cell via an air pressure-

565 driven (MPCU, Lorenz Meßgerätebau, Katlenburg-Lindau, Germany) application

566 pipette. All solutions revealed an osmolality of 290 to 310 mOsm. Every 2 s voltage

567 ramps of 50 ms duration spanning from -100 mV to +100 mV were applied from a

568 holding potential (V_h) of 0 mV using the PatchMaster software (HEKA). All voltages

569 were corrected for a liquid junction potential of 10 mV and currents were filtered at

570 2.9 kHz and digitized at 100 µs intervals. Before each voltage ramp, capacitive

571 currents and series resistance were determined and corrected by the EPC9 automatic

572 capacitance compensation. Inward and outward currents at -80 and +80 mV were

573 extracted from each individual ramp current recording and amplitudes were plotted

574 versus time. Current-voltage (IV) relationships were extracted at indicated time points.

575 To obtain the net developing current (I_{net}), basic currents (I_{min}) were subtracted from

576 single IVs. All currents were normalized to the initial size i.e. capacitance of the cell to

577 obtain current densities (pA/pF).

578 ***Morphological Analysis.*** Standard hematoxylin and eosin staining on 10 µm

579 cryosections of islets and immunofluorescence staining of whole islets were performed

580 to assess pancreatic islet morphology. Antibodies and their working dilutions are listed

581 in Supplemental Table 3. Digital imaging fluorescence microscopy of the pancreas was

582 performed using a scanning platform (MetaSystems) with a Zeiss Imager Z.2

583 microscope (Carl Zeiss MicroImaging, Inc.). Quantitative image analysis of islet

584 morphology was performed using ImageJ. β-cell size was measured by imaging

585 randomly selected cells at 400X. β-cell size was determined as mean individual β-cell

586 cross-sectional area for at least 5 islets per animal using ImageJ software. For the

587 mean individual β-cell cross-sectional area, the insulin-positive area of each islet was

588 divided by the number of nuclei within the insulin-positive area. Investigators were

589 blinded during analysis.

590 ***Western Blot.*** Western blot analysis was performed as previously described (63).

591 Twenty µg of protein were loaded, resolved on 8-12% Tris-HCl SDS-PAGE gel and

592 blotted onto a nitrocellulose membrane (Amersham Biosciences, Freiburg, Germany).

593 Membranes were blocked for 1 hour using 5% bovine serum albumin or nonfat dried

594 milk diluted in Tris-buffered saline with 0.1% Tween® 20 detergent (TBST) at room

595 temperature and incubated with primary antibodies (Supplemental Table 3) at 4 °C for

596 16 hours. After washing, membranes were incubated with HRP-conjugated secondary

597 antibodies (Supplemental Table 3) for 1 hour at room temperature. Immunobound

598 antibody was visualized with an enhanced chemiluminescence kit (GE Healthcare

599 Europe, Freiburg, Germany). ChemiDoc MP Imaging System (BioRad) was used for

600 chemiluminescence detection. For the loading control, membranes were stripped and

601 incubated with an antibody against ERK2 or Histon H3 for approximately 16hours at

602 4 °C.

603 ***RNA Isolation.*** RNA was extracted from pancreatic islets using the RNeasy Mini Kit

604 (Qiagen), following the manufacturer's instructions. cDNA was prepared using

605 QuantiTect Reverse Transcription Kit (Qiagen), according to the manufacturer's

606 protocol.

607 **Quantitative RT-PCR.** Real-time PCR was performed in triplicate with a Bio-Rad

608 iCycler by cycling 40 times using the following conditions: 95 °C for 10 s, 60 °C for

609 45 s. Primers were designed using Primer3 as above and tested for linear amplification

610 using serial dilutions of cDNA before use on experimental samples. Sequence

611 information is provided in Supplemental Table 4.

Measurement of β-cell Proliferation and Apoptosis. Pancreatic slices were prepared from *Trpm7R/R* and control littermates after 16-wks of chow or HFD. To study β-cell proliferation, pancreatic islets were co-stained for insulin and Ki67. Ki67-insulin double-positive cells were counted and divided by the total number of insulin-positive cells per pancreatic section. To investigate β-cell apoptosis, ApopTag® Red In Situ Apoptosis Detection Kit was used according to the manufacturer's (Merk) instructions. TUNEL-insulin double-positive cells were counted and divided by the total number of insulin-positive cells per pancreatic section.

RNA-seq studies. RNA-seq data have been uploaded to GEO under the accession number GSE218030 (https://www.ncbi.nlm.nih.gov/geo). Total RNA was extracted from isolated pancreatic islets of *Trpm7R/R* and their control littermates, which had been maintained on a HFD for 16-wks. Template amplification and clustering were performed onboard of the NovaSeq 6000 applying the exclusion amplification (ExAmp) chemistry. The ExAmp workflow is a proprietary Illumina method and ensures that only single DNA templates are bound within single wells of the patterned NovaSeq flow cells and are almost instantaneously amplified. Cluster generation and sequencing were operated under the control of the NovaSeq Control Software (NVCS) v1.6.0. The *P* value of a pairwise comparison was derived from the Wald test. To control the false positive rate, FDR-corrected (64) as well as Bonferroni-corrected *P* values were calculated, where FDR is the proportion of false positive hits among all positive hits. A gene or transcript is classified as upregulated or downregulated in a specific comparison if its FDR-corrected *P* value is ≤ 0.05 and its fold change is ≥ 2.

Bio-Plex Pro™ Cell Signaling Assay. Murine pancreatic islets were washed and lysed in MILLIPLEX® MAP Lysis Buffer. Protein content was measured using Pierce™ BCA Protein Assay Kit (Thermo Scientific™, catalog #23225). Samples were stored at

637 −80 °C. Collected samples were processed and assayed according to manufacturer's

638 instructions specific for MILLIPLEX MAP TGFβ Signaling Pathway Magnetic Bead 6-

639 Plex kit (Merck, catalog #48-614MAG), and MILLIPLEX MAP β-Tubulin Total Magnetic

640 Bead MAPmate™ (Merck, catalog #46-713MAG).

641 **Cell culture.** Mouse WT and kinase-dead TRPM7 in pIRES-EGFP vector were

642 reported previously (65). MIN6 cells were generously provided by Prof. Per-Olof

643 Berggren and Dr. Barbara Leibiger, Karolinska Institute, Stockholm, Sweden. MIN6

644 cells were grown at 37 °C and 5% CO_2 in Dulbecco's modified Eagle's medium

645 (DMEM, Sigma-Aldrich) supplemented with 10% fetal bovine serum (FBS, Thermo

646 Fisher Scientific), 100 U/ml penicillin and 100 µg/ml streptomycin (Sigma-Aldrich) and

647 75 µM ß-Mercaptoethanol (Gibco). Cells ~60% confluence in 96-well plates or 6 cm

648 dishes were transiently transfected by 0.1 or 2 µg cDNAs, respectively. TurboFect™

649 was used as a transfection reagent (Thermo Fisher Scientific). GIIS was measured

650 48 hours after transfection in 96-well plates. Cells were harvested 48 hours after

651 transfection from 6 cm dishes for western blotting.

652 **Statistics.** Data were expressed as mean ± S.E.M. *P* value less than 0.05 was

653 considered significant. Graph presentations, curve fittings, statistics, and *P* values

654 were obtained by Prism software (version 9.0.1; GraphPad). For comparison of two

655 groups, *P* values were calculated by the unpaired two-tailed Student´s t-test for

656 parametric or Mann-Whitney test for non-parametric distribution. For three and more

657 groups, one-way ANOVA with Bonferroni multiple comparison were used for

658 parametrically distributed data. Glucose and insulin tolerance tests were compared

659 using two-way ANOVA with Bonferroni multiple comparison.

Author contribution. NK designed and conducted experiments, analyzed, and interpreted data, prepared figures, and wrote the manuscript. A. Beck, KR, PB, KJ, SFS, A. Belkacemi, PCFS, HS, TP, conducted experiments, analyzed, and interpreted data, and edited the manuscript. PSR, AN, A. Breit, VC, TDM, SZ interpreted data, and edited the manuscript. TG directed the project, designed experiments, interpreted data, and edited the manuscript.

28

687

References

689 1.   Prentki M, Nolan CJ. Islet beta cell failure in type 2 diabetes. *JCI Insight*. 2006;116(7):1802-12.

690 2.   Schmitz C, et al. Regulation of vertebrate cellular Mg2+ homeostasis by TRPM7. *Cell*.
691   2003;114(2):191-200.

692 3.   Mittermeier L, et al. TRPM7 is the central gatekeeper of intestinal mineral absorption essential
693   for postnatal survival. *Proc Natl Acad Sci U S A*. 2019;116(10):4706-15.

694 4.   Pham PC, et al. Hypomagnesemia in patients with type 2 diabetes. *Clin J Am Soc Nephrol*.
695   2007;2(2):366-73.

696 5.   Rodríguez-Morán M, Guerrero-Romero F. Oral magnesium supplementation improves insulin
697   sensitivity and metabolic control in type 2 diabetic subjects: a randomized double-blind
698   controlled trial. *Diabetes Care*. 2003;26(4):1147-52.

699 6.   Ryazanov AG. Elongation factor-2 kinase and its newly discovered relatives. *FEBS Lett*.
700   2002;514(1):26-9.

701 7.   Zierler S, et al. TRPM channels as potential therapeutic targets against pro-inflammatory
702   diseases. *Cell calcium*. 2017;67:105-15.

703 8.   Drennan D, Ryazanov AG. Alpha-kinases: analysis of the family and comparison with
704   conventional protein kinases. *Prog Biophys Mol Biol*. 2004;85(1):1-32.

705 9.   Riazanova LV, et al. Signal'nye molekuly novogo tipa: proteinkinazy, kovalentno sviazannye s
706   ionnymi kanalami. [Novel type of signaling molecules: protein kinases covalently linked to ion
707   channels]. *Mol Biol (Mosk)*. 2001;35(2):321-32.

708 10.   Yamaguchi H, et al. Crystal structure of the atypical protein kinase domain of a TRP channel
709   with phosphotransferase activity. *Mol Cell*. 2001;7(5):1047-57.

710 11.   Jin J, et al. The channel kinase, TRPM7, is required for early embryonic development. *Proc Natl*
711   *Acad Sci U S A*. 2012;109(5):E225-33.

712 12.   Yu Y, et al. TRPM7 is involved in angiotensin II induced cardiac fibrosis development by
713   mediating calcium and magnesium influx. *Cell Calcium*. 2014;55(5):252-60.

714 13.   Sahni J, Scharenberg AM. TRPM7 ion channels are required for sustained phosphoinositide 3-
715   kinase signaling in lymphocytes. *Cell Metab*. 2008;8(1):84-93.

716 14.   Fang L, et al. TRPM7 channel regulates PDGF-BB-induced proliferation of hepatic stellate cells
717   via PI3K and ERK pathways. *Toxicol Appl Pharmacol*. 2013;272(3):713-25.

718 15.   Sahni J, et al. TRPM7 regulates quiescent/proliferative metabolic transitions in lymphocytes.
719   *Cell Cycle*. 2010;9(17):3565-74.

720 16.   Yee NS, et al. Transient receptor potential ion channel Trpm7 regulates exocrine pancreatic
721   epithelial proliferation by Mg2+-sensitive Socs3a signaling in development and cancer. *Dis*
722   *Model Mech*. 2011;4(2):240-54.

723 17.   Krapivinsky G, et al. The TRPM7 chanzyme is cleaved to release a chromatin-modifying kinase.
724   *Cell*. 2014;157(5):1061-72.

725 18.   Abed E, Moreau R. Importance of melastatin-like transient receptor potential 7 and
726   magnesium in the stimulation of osteoblast proliferation and migration by platelet-derived
727   growth factor. *Am J Physiol Cell Physiol*. 2009;297(2):C360-8.

728 19.   Beesetty P, et al. Inactivation of TRPM7 kinase in mice results in enlarged spleens, reduced T-
729   cell proliferation and diminished store-operated calcium entry. *Sci Rep*. 2018;8(1):3023.

730 20.   Faouzi M, et al. The TRPM7 channel kinase regulates store-operated calcium entry. *J Physiol*.
731   2017;595(10):3165-80.

732 21. Altman MK, et al. TRPM7 is a crucial regulator of pancreatic endocrine development and high-
733   fat-diet-induced β-cell proliferation. *Development*. 2021;148(16).
734 22. Kono T, et al. Impaired Store-Operated Calcium Entry and STIM1 Loss Lead to Reduced Insulin
735   Secretion and Increased Endoplasmic Reticulum Stress in the Diabetic β-Cell. *Diabetes*.
736   2018;67(11):2293-304.
737 23. Islam MS. Molecular Regulations and Functions of the Transient Receptor Potential Channels
738   of the Islets of Langerhans and Insulinoma Cells. *Cells*. 2020;9(3).
739 24. Gommers LMM, et al. Low extracellular magnesium does not impair glucose-stimulated insulin
740   secretion. *PLoS One*. 2019;14(6):e0217925.
741 25. Sachdeva MM, et al. Pdx1 (MODY4) regulates pancreatic beta cell susceptibility to ER stress.
742   *Proc Natl Acad Sci U S A*. 2009;106(45):19090-5.
743 26. Wang P, et al. Diabetes mellitus--advances and challenges in human β-cell proliferation. *Nat
744   Rev Endocrinol*. 2015;11(4):201-12.
745 27. Golson ML, et al. High Fat Diet Regulation of β-Cell Proliferation and β-Cell Mass. *Open
746   Endocrinol J*. 2010;4.
747 28. Romagnani A, et al. TRPM7 kinase activity is essential for T cell colonization and alloreactivity
748   in the gut. *Nat Commun*. 2017;8(1):1917.
749 29. Zhang Y, et al. TGF-β Family Signaling in the Control of Cell Proliferation and Survival. *Cold
750   Spring Harb Perspect Biol*. 2017;9(4).
751 30. Melloul D, Marshak S, Cerasi E. Regulation of pdx-1 gene expression. *Diabetes*. 2002;51 Suppl
752   3:S320-5.
753 31. Seufert J, et al. Differential expression of the insulin gene transcriptional repressor
754   CCAAT/enhancer-binding protein beta and transactivator islet duodenum homeobox-1 in rat
755   pancreatic beta cells during the development of diabetes mellitus. *J Clin Invest*.
756   1998;101(11):2528-39.
757 32. Ahn YB, et al. Changes in gene expression in beta cells after islet isolation and transplantation
758   using laser-capture microdissection. *Diabetologia*. 2007;50(2):334-42.
759 33. Chakrabarti SK, et al. Quantitative assessment of gene targeting in vitro and in vivo by the
760   pancreatic transcription factor, Pdx1. Importance of chromatin structure in directing promoter
761   binding. *J Biol Chem*. 2002;277(15):13286-93.
762 34. Ohlsson H, et al. IPF1, a homeodomain-containing transactivator of the insulin gene. *EMBO J*.
763   1993;12(11):4251-9.
764 35. Moin ASM, Butler AE. Alterations in Beta Cell Identity in Type 1 and Type 2 Diabetes. *Curr Diab
765   Rep*. 2019;19(9):83.
766 36. Guo S, et al. Inactivation of specific β cell transcription factors in type 2 diabetes. *J Clin Invest*.
767   2013;123(8):3305-16.
768 37. Hayes HL, et al. Pdx-1 activates islet α- and β-cell proliferation via a mechanism regulated by
769   transient receptor potential cation channels 3 and 6 and extracellular signal-regulated kinases
770   1 and 2. *Mol Cell Biol*. 2013;33(20):4017-29.
771 38. Reers C, et al. Impaired islet turnover in human donor pancreata with aging. *Eur J Endocrinol*.
772   2009;160(2):185-91.
773 39. Kulkarni RN, et al. PDX-1 haploinsufficiency limits the compensatory islet hyperplasia that
774   occurs in response to insulin resistance. *J Clin Invest*. 2004;114(6):828-36.
775 40. Chubanov V, et al. Role of kinase-coupled TRP channels in mineral homeostasis. *Pharmacol
776   Ther*. 2018;184:159-76.
777 41. Rane SG, et al. Loss of Cdk4 expression causes insulin-deficient diabetes and Cdk4 activation
778   results in beta-islet cell hyperplasia. *Nat Genet*. 1999;22(1):44-52.
779 42. Kim SY, Rane SG. The Cdk4-E2f1 pathway regulates early pancreas development by targeting
780   Pdx1+ progenitors and Ngn3+ endocrine precursors. *Development*. 2011;138(10):1903-12.
781 43. Lee JH, et al. Cdk4 regulates recruitment of quiescent beta-cells and ductal epithelial
782   progenitors to reconstitute beta-cell mass. *PLoS One*. 2010;5(1):e8653.

783   44.   Masuda T, et al. Cold-inducible RNA-binding protein (Cirp) interacts with Dyrk1b/Mirk and
784   promotes proliferation of immature male germ cells in mice. *Proc Natl Acad Sci U S A*.
785   2012;109(27):10885-90.
786   45.   Laybutt DR, et al. Endoplasmic reticulum stress contributes to beta cell apoptosis in type 2
787   diabetes. *Diabetologia*. 2007;50(4):752-63.
788   46.   Barella LF, et al. β-Arrestin-1 is required for adaptive β-cell mass expansion during obesity. *Nat*
789   *Commun*. 2021;12(1):3385.
790   47.   Johnson JS, Kono T, et al. Pancreatic and duodenal homeobox protein 1 (Pdx-1) maintains
791   endoplasmic reticulum calcium levels through transcriptional regulation of sarco-endoplasmic
792   reticulum calcium ATPase 2b (SERCA2b) in the islet β cell. *J Biol Chem*. 2014;289(47):32798-
793   810.
794   48.   Elrick LJ, Docherty K. Phosphorylation-dependent nucleocytoplasmic shuttling of pancreatic
795   duodenal homeobox-1. *Diabetes*. 2001;50(10):2244-52.
796   49.   Jara MA, et al. Pancreatic and duodenal homeobox-1 (PDX1) contributes to β-cell mass
797   expansion and proliferation induced by Akt/PKB pathway. *Islets*. 2020;12(2):32-40.
798   50.   Khoo S, et al. Regulation of insulin gene transcription by ERK1 and ERK2 in pancreatic beta cells.
799   *J Biol Chem*. 2003;278(35):32969-77.
800   51.   Huang X, et al. The PI3K/AKT pathway in obesity and type 2 diabetes. *Int J Biol Sci*.
801   2018;14(11):1483-96.
802   52.   Bernal-Mizrachi E, et al. Islet beta cell expression of constitutively active Akt1/PKB alpha
803   induces striking hypertrophy, hyperplasia, and hyperinsulinemia. *J Clin Invest*.
804   2001;108(11):1631-8.
805   53.   Tuttle RL, et al. Regulation of pancreatic beta-cell growth and survival by the serine/threonine
806   protein kinase Akt1/PKBalpha. *Nat Med*. 2001;7(10):1133-7.
807   54.   Kitamura T, et al. The forkhead transcription factor Foxo1 links insulin signaling to Pdx1
808   regulation of pancreatic beta cell growth. *J Clin Invest*. 2002;110(12):1839-47.
809   55.   Roy SK, et al. Inhibition of PI3K/AKT and MAPK/ERK pathways causes activation of FOXO
810   transcription factor, leading to cell cycle arrest and apoptosis in pancreatic cancer. *J Mol Signal*.
811   2010;5:10.
812   56.   Kim TK, et al. Triiodothyronine induces proliferation of pancreatic β-cells through the
813   MAPK/ERK pathway. *Exp Clin Endocrinol Diabetes*. 2014;122(4):240-5.
814   57.   Stewart AF, et al. Human β-cell proliferation and intracellular signaling: part 3. *Diabetes*.
815   2015;64(6):1872-85.
816   58.   Nadolni W, et al. TRPM7 Kinase Is Essential for Neutrophil Recruitment and Function via
817   Regulation of Akt/mTOR Signaling. *Front Immunol*. 2020;11:606893.
818   59.   Fatrai S, et al. Akt induces beta-cell proliferation by regulating cyclin D1, cyclin D2, and p21
819   levels and cyclin-dependent kinase-4 activity. *Diabetes*. 2006;55(2):318-25.
820   60.   Jin J, et al. Deletion of Trpm7 disrupts embryonic development and thymopoiesis without
821   altering Mg2+ homeostasis. *Science*. 2008;322(5902):756-60.
822   61.   Kaitsuka T, et al. Inactivation of TRPM7 kinase activity does not impair its channel function in
823   mice. *Sci Rep*. 2014;4:5718.
824   62.   Khajavi N, et al. An incretin-based tri-agonist promotes superior insulin secretion from murine
825   pancreatic islets via PLC activation. *Cell Signal*. 2018;51:13-22.
826   63.   Khajavi N, et al. L-carnitine reduces in human conjunctival epithelial cells hypertonic-induced
827   shrinkage through interacting with TRPV1 channels. *Cell Physiol Biochem*. 2014;34(3):790-803.
828   64.   Benjamini Y, Hochberg Y. Controlling the false discovery rate: a practical and powerful
829   approach to multiple testing. *J R Stat Soc Series B Stat Methodol*. 1995;57(1):289-300.
830   65.   Schmidt E, et al. Structural mechanism of TRPM7 channel regulation by intracellular
831   magnesium. *Cell Mol Life Sci*. 2022;79(5):225.

832

833
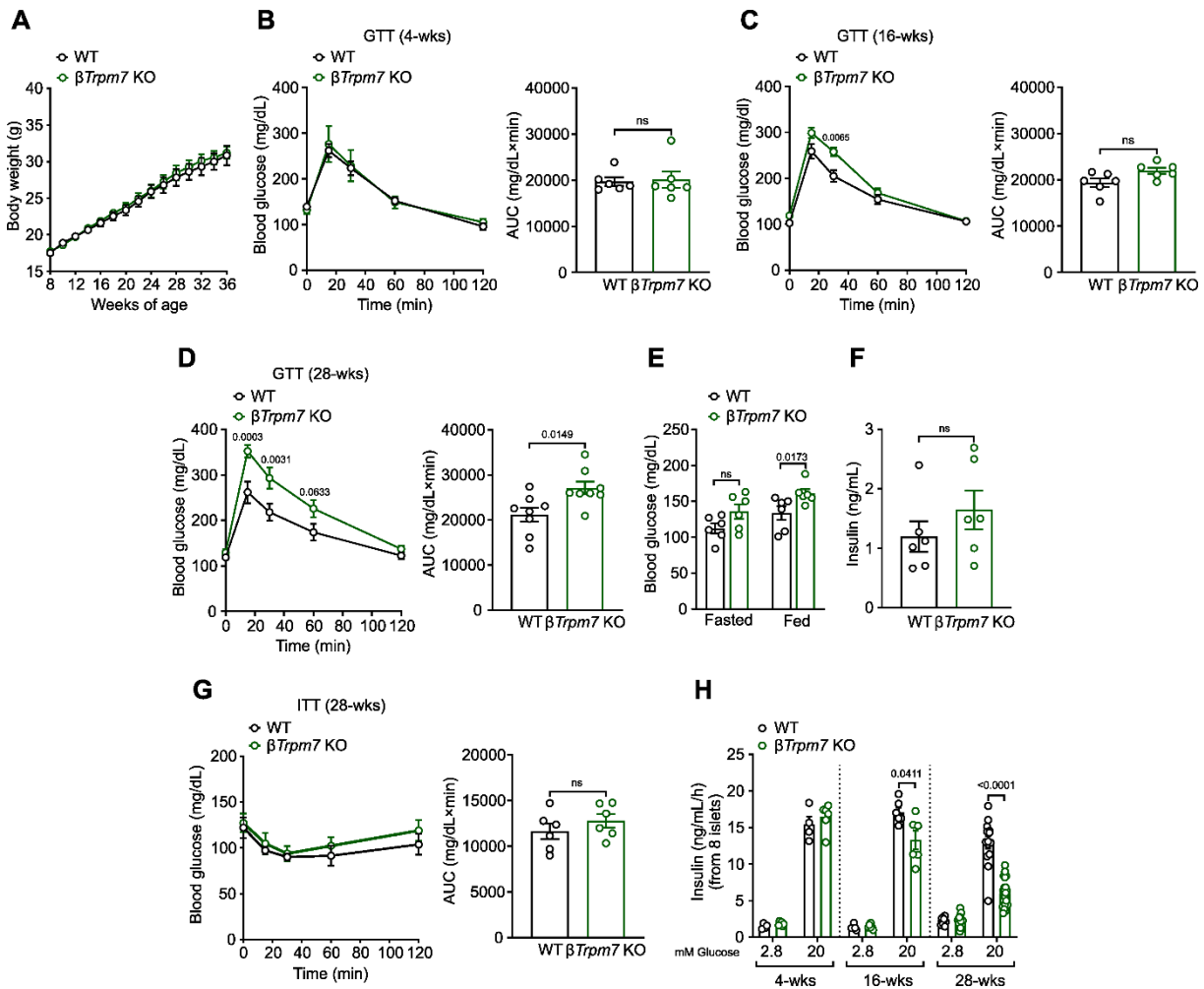
Figure 1 Tissue-specific TRPM7 deletion in β-cells impairs glucose homeostasis and glucose-induced insulin secretion. (**A**) Body weight development for 36-wks (n = 6 mice per genotype) monitored in male β$Trpm7$ KO and control littermate on chow diet. (**B-D**) For glucose tolerance test (GTT) mice were fasted overnight (n = 6 mice per genotype). Blood glucose levels (mg/dL) before and within 2 hours after i.p. injection of glucose (2 g/kg of body weight) in WT and β$Trpm7$ KO mice (left panels) and area under the curves (AUC in mg/dL × min; right panels) after 4- (B), 16- (C) and 28-wks (D) post-recombination. (**E**) Blood glucose (mg/dL) in freely fed (n = 6 per genotype) or fasted (n = 6 mice per genotype) and (**F**) plasma insulin levels (ng/mL) in freely fed (n = 6 mice per genotype) were measured in 36-wks old β$Trpm7$ KO and control littermate. (**G**) For insulin tolerance test (ITT) mice were fasted for 4 hours at the onset of the light cycle (n = 6 mice per genotype). Blood glucose levels (mg/dL) before and within 2 hours after i.p. injection of insulin (0.75 U/kg of body weight) in WT and β$Trpm7$ KO mice (left panels) and AUC (mg/dL × min; right panels). (**H**) Insulin secretion (ng/mL/h/8 islets) in isolated islets of male β$Trpm7$ KO and control littermate mice 4-, 16- and 28-wks post-recombination. Islets were incubated for 1 hour in the presence of low glucose and high glucose (n ≥ 3 mice per genotype, measured in duplicate). Data show means ± S.E.M., and statistical differences were assessed by two-way ANOVA (B left-D left, G left) or unpaired two-tailed Student's t-test (B right-D right, E, F, G right, H). Circles in bar graphs represent single values. P values are shown above the bars. (ns, not significant)
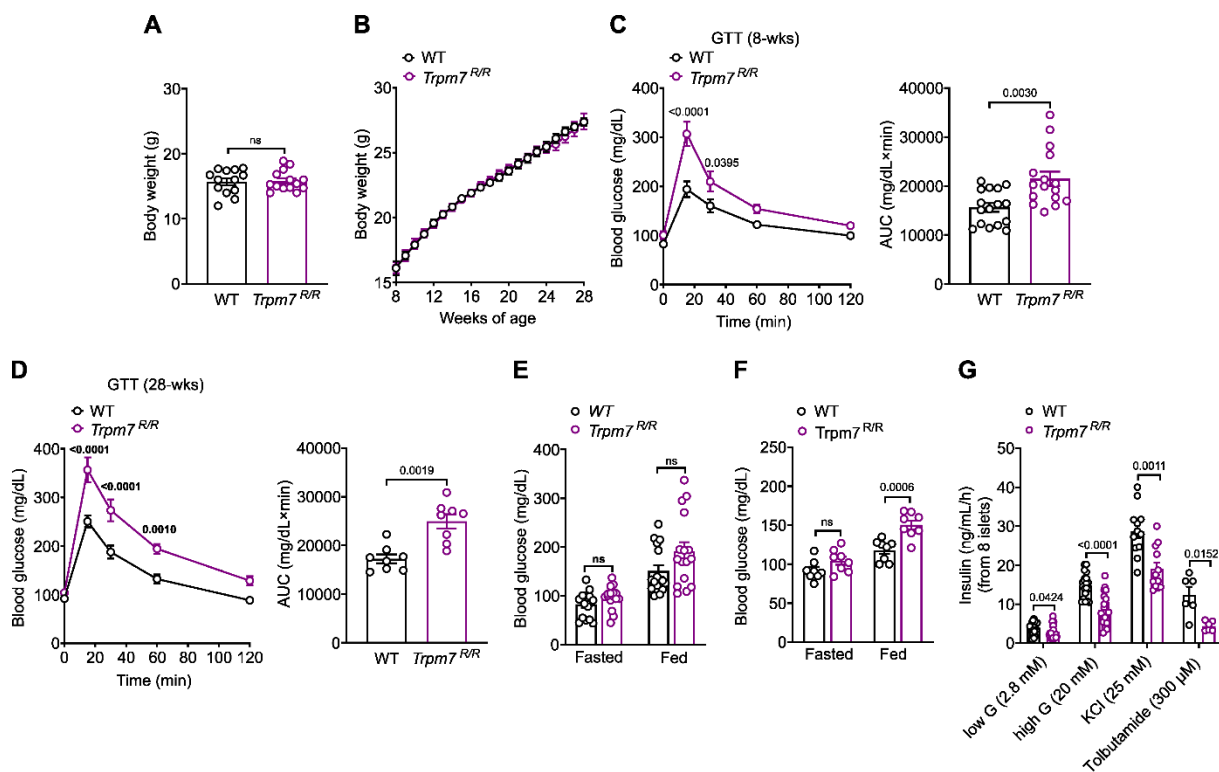
Figure 2 TRPM7 kinase disruption impairs glucose homeostasis and glucose-induced insulin secretion. (**A** and **B**) Body weight at 8- to 9-wks ($n \geq 14$ mice per genotype) (A) and its development for 28-wks ($n = 10$ mice per genotype) (B) monitored in male and female $Trpm7^{R/R}$ and control littermate mice on chow diet. (**C, D**) Blood glucose levels (mg/dL) before and within 2 hours after i.p. injection of glucose (2 g/kg of body weight) and in WT and $Trpm7^{R/R}$ mice (left panels) and area under the curves (AUC in mg/dL × min; right panels) at age of 8- 9-wks (C) and 28-wks (D). For glucose tolerance test (GTT) mice were fasted overnight ($n = 16$ mice per genotype ($n \geq 8$ mice per genotype). (**E, F**) Blood glucose (mg/dL) in freely fed ($n \geq 8$ per genotype) or fasted (n $\geq$ 8 mice per genotype) were measured in $Trpm7^{R/R}$ and control littermate mice at age of 8- 9-wks (E) and 28-wks (F). (**G**) Insulin secretion (ng/mL/h/8 islets) in isolated islets of male and female $Trpm7^{R/R}$ and control littermate mice at 8-wks of age. Islets were incubated for 1 hour in the presence of low glucose (2.8 mM), high glucose (20 mM), 25 mM KCl or 300 µM tolbutamide (n $\geq$ 3 mice per genotype, measured in duplicate). Data show means ± S.E.M., and statistical differences were assessed by unpaired two-tailed Student's t-test (A, C right, D right, E-G) or two-way ANOVA (C left, D left). Circles in bar graphs represent single values. *P* values are shown above the bars. (ns, not significant)

33
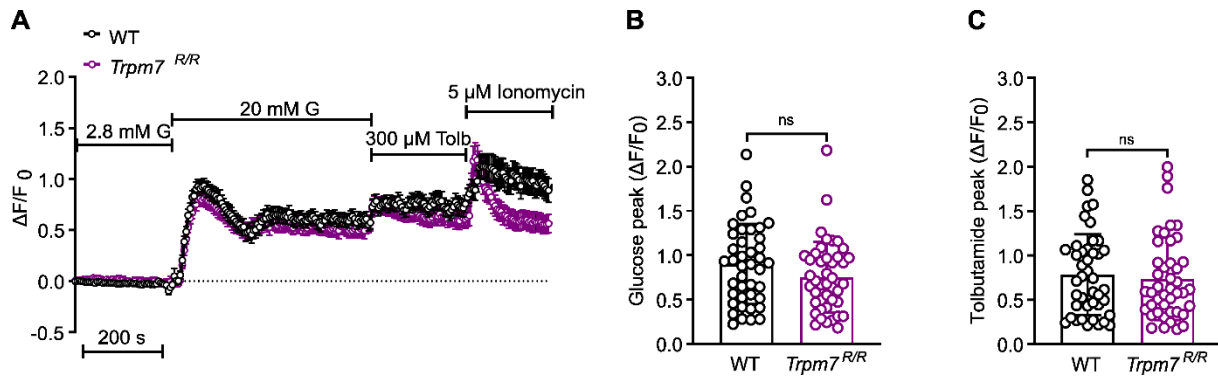
Figure 3 TRPM7 kinase disruption has no effect on glucose-induced Ca^{2+} responses (**A**) Intact WT ($n = 42$ cells, from 3 mice) and *Trpm7$^{R/R}$* ($n = 43$, from 3 mice) islets were loaded with 4 µM fluo-4 AM and alterations in $[Ca^{2+}]_i$ of individual cells were monitored by confocal microscopy after increasing the extracellular glucose concentration from 2.8 to 20 mM and application of 300 µM tolbutamide. Ionomycin (5 µM) was used as a positive control. (**B** and **C**) Average of Ca^{2+} influx peaks assessed from baseline after glucose (B) and tolbutamide (C) stimulation in WT and *Trpm7$^{R/R}$* β-cells. The cells which displayed no increase in $[Ca^{2+}]_i$ in response to high glucose concentration are excluded from the results. Data are given as means ± S.E.M. (circles in bar graphs represent single values) and statistical differences were assessed by unpaired two-tailed Student's t-test (B, C). (ns, not significant)
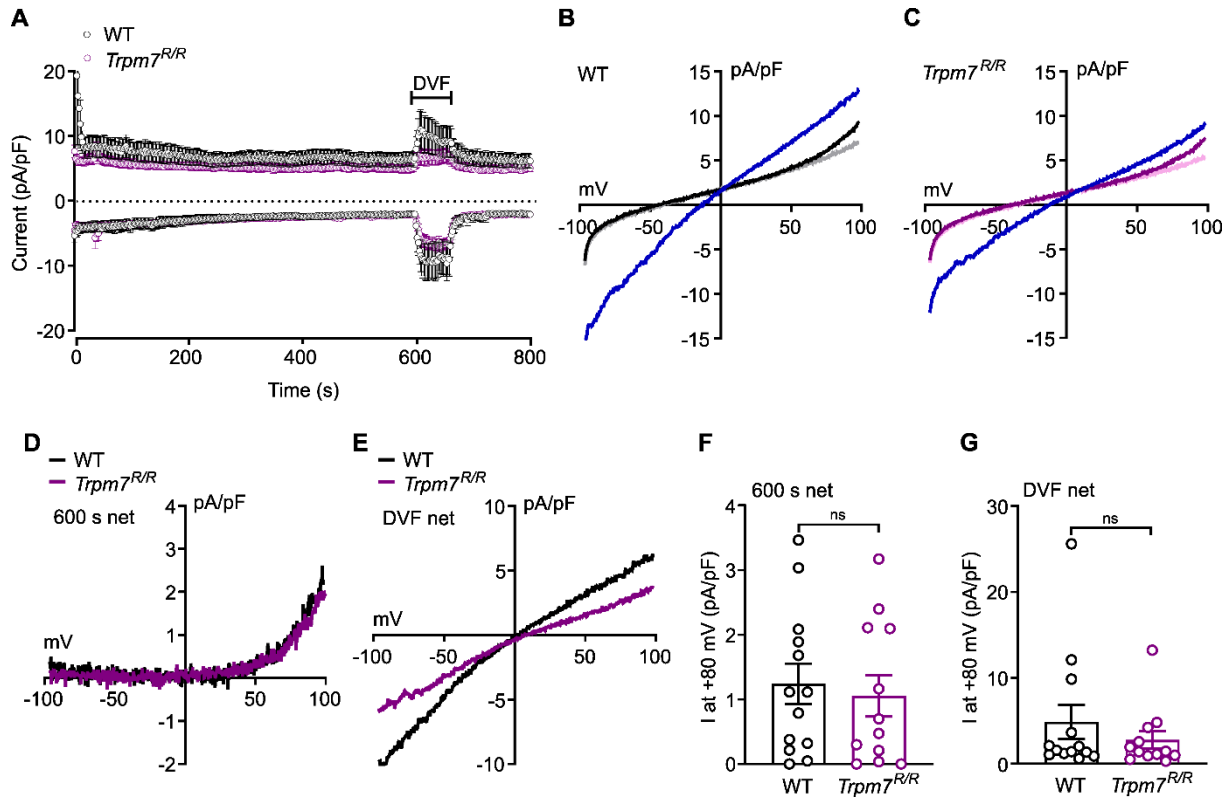
Figure 4 TRPM7 kinase inactivation has no effect on TRPM7 current activity Whole-cell currents recorded from islet cells of WT (**A, D, E** black trace, **B**) and *Trpm7$^{R/R}$* mice (**A, D, E** purple trace, **C**), using Mg^{2+}-free pipette solution (buffered by 10 mM EDTA). (**A**) In- and outward current amplitudes at -80 mV (lower traces) and +80 mV (upper traces), extracted from whole-cell currents mediated by voltage ramps, applied at 0.5 Hz, spanning from -100 mV to 100 mV within 50 ms, in the absence of intracellular Mg^{2+} in WT and *Trpm7$^{R/R}$* islet cells, plotted versus time. Divalent-free solution (DVF, buffered by EDTA) was applied from 600 s to 660 s (bar). (**B** and **C**) Current-voltage relationships (IVs) of the minimal basic current (grey, light purple), the current at 600 s (black, purple, right before DVF) and in DVF solution (blue) in WT (B) and in *Trpm7$^{R/R}$* islet cells (C). (**D** and **E**) IVs of the net current at 600 s (600 s net = current at 600 s minus basic current) and in DVF solution (DVF net = current in DVF minus basic current) in WT (black) and *Trpm7$^{R/R}$* islet cells (purple). (**F** and **G**) Summary of the net current amplitudes at +80 mV from IVs at 600 s (600 s net; F) and in DVF solution (DVF net; G) in cells isolated from WT (black) and *Trpm7$^{R/R}$* mice (purple). All currents were normalized to the cell capacitance (pA/pF). Data are plotted as means ± S.E.M (A, F, G) or means (B-E)**.** Data are from 13 cells for WT and 12 cells for *Trpm7$^{R/R}$*. Data are given as means ± S.E.M. (circles in bar graphs represent single values) and statistical differences were assessed by unpaired two-tailed Student's t-test (F, G). (ns, not significant)

914
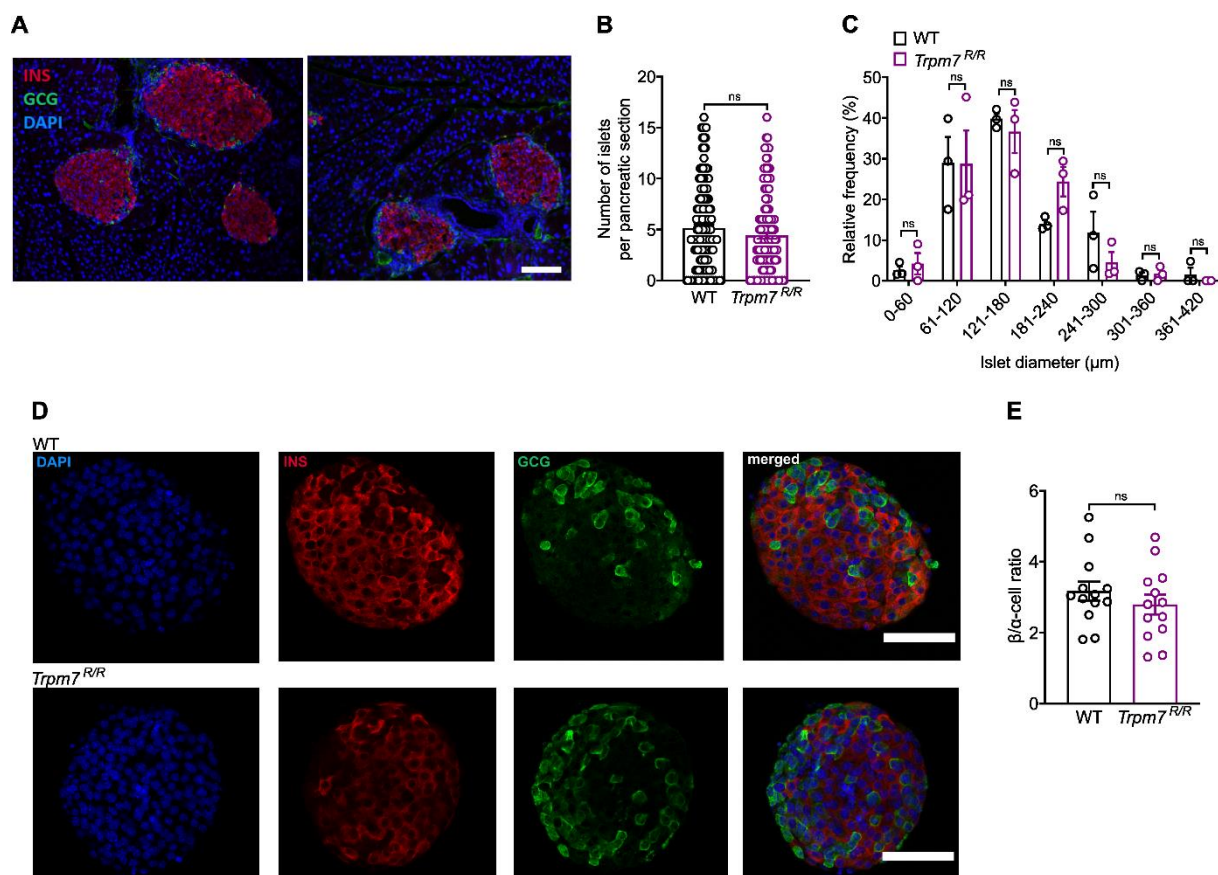
Figure 5 Morphology of WT and *Trpm7^R/R* pancreatic islets. (**A**) Immunofluorescent insulin (INS, red) and glucagon (GCG, green) staining of pancreatic cryosections of WT and *Trpm7^R/R* mice. Nuclei were stained with DAPI (blue) and scale bars represent 100 µm. (**B**) Number of islets per pancreatic cryosection (*n* = 140 slides, 3 mice per genotype) and (**C**) relative frequency plot of islet diameter comparing WT with *Trpm7^R/R* islets (*n* = 140 slides, 3 mice per genotype). (**D**) Confocal images of WT and *Trpm7^R/R* islets stained for insulin (INS, β-cells, red), glucagon (GCG, α-cells, green). Nuclei were stained with DAPI (blue) and scale bars represent 100 µm. (**E**) Quantification of the ratio of the number of β- and α-cells per pancreatic islet in WT and *Trpm7^R/R* mice (*n* = 13, 3 mice per genotype). Data are given as means ± S.E.M. (circles in bar graphs represent single values) and statistical differences were assessed by Mann-Whitney test (B) and unpaired two-tailed Student's t-test (C, E). (ns, not significant)

925

926

927

928

929

930

931

932

933

934

935
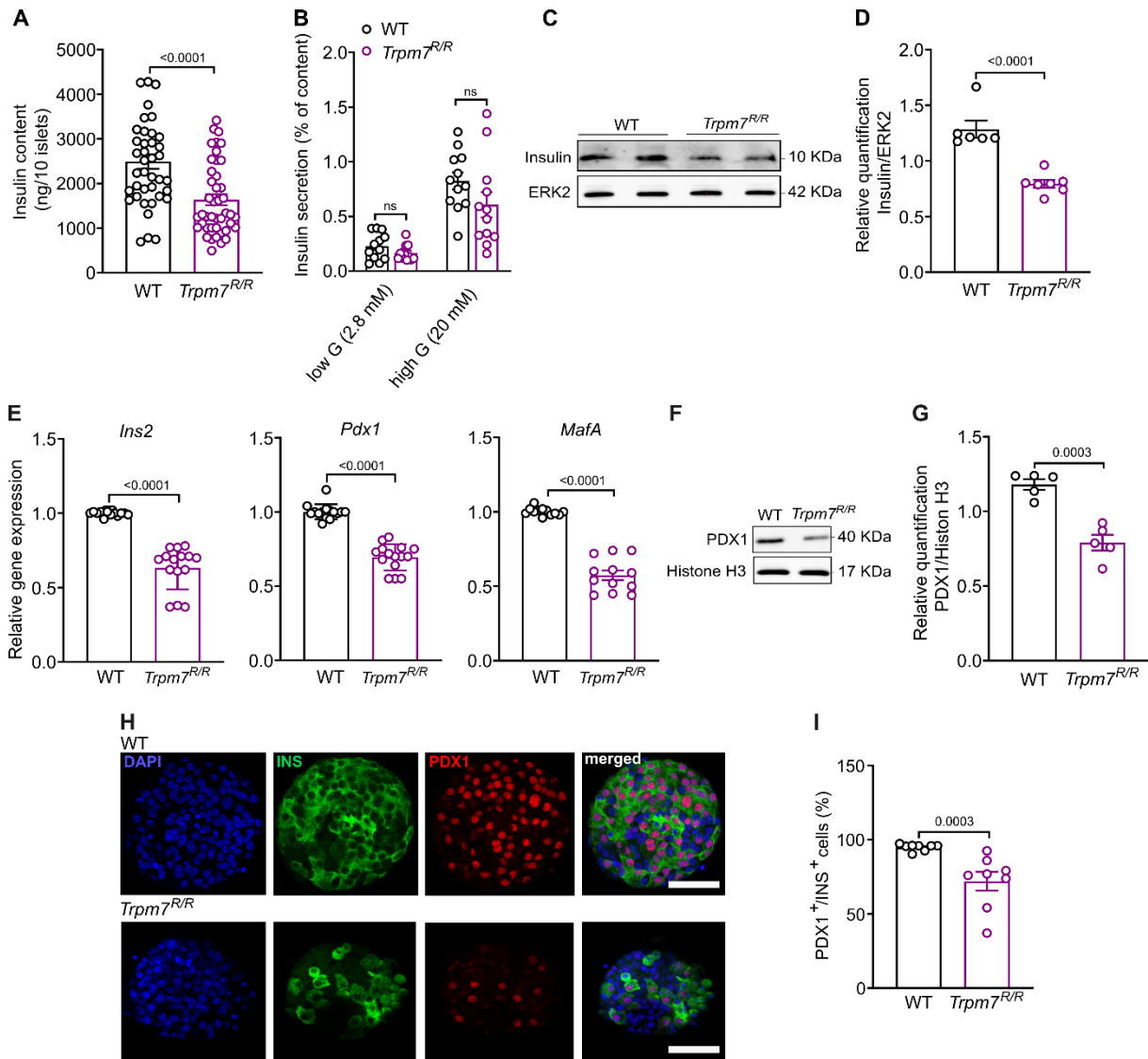
Figure 6 TRPM7 kinase disruption impairs insulin production. (**A**) Total insulin content of pooled WT versus *Trpm7^{R/R}* islets. At least 40 groups of 10 size-matched WT and *Trpm7^{R/R}* islets were compared. (**B**) Percent of insulin content secreted from intact WT or *Trpm7^{R/R}* islets after incubation with either low glucose (2.8 mM) or high glucose (20 mM) ($n = 6$ mice per genotype, measured in duplicate). (**C** and **D**) Western blot detection of the insulin in lysates of purified islets from WT and *Trpm7^{R/R}* mice ($n \geq 5$, 4 mice per genotype). Insulin was normalized to ERK2 as loading control. (**E**) Expression levels of *Ins2*, *Pdx1*, and *MafA* analyzed by qRT-PCR from RNAs isolated from pancreatic islet from WT and *Trpm7^{R/R}* mice. (**F** and **G**) Western blot detection of the PDX1 in lysates of purified islets from WT and *Trpm7^{R/R}* mice ($n = 4$, 4 mice per genotype). PDX1 was normalized to Histone H3 as loading control. (**H**) Confocal images of WT and *Trpm7^{R/R}* islets stained for DAPI (blue), insulin (green), PDX1 (red). The scale bar represents 100 μm. (**I**) Percentage of PDX1-positive cells from the population (100%) of insulin-positive cells per pancreatic islet in WT and *Trpm7^{R/R}* mice ($n = 8$, 4 mice per genotype). Data are given as means ± S.E.M. (circles in bar graphs represent single values) and statistical differences were assessed by Mann-Whitney test (A) or unpaired two-tailed Student's t-test (B, D, E, G, I). *P* values are shown above the bars. (ns, not significant)

951
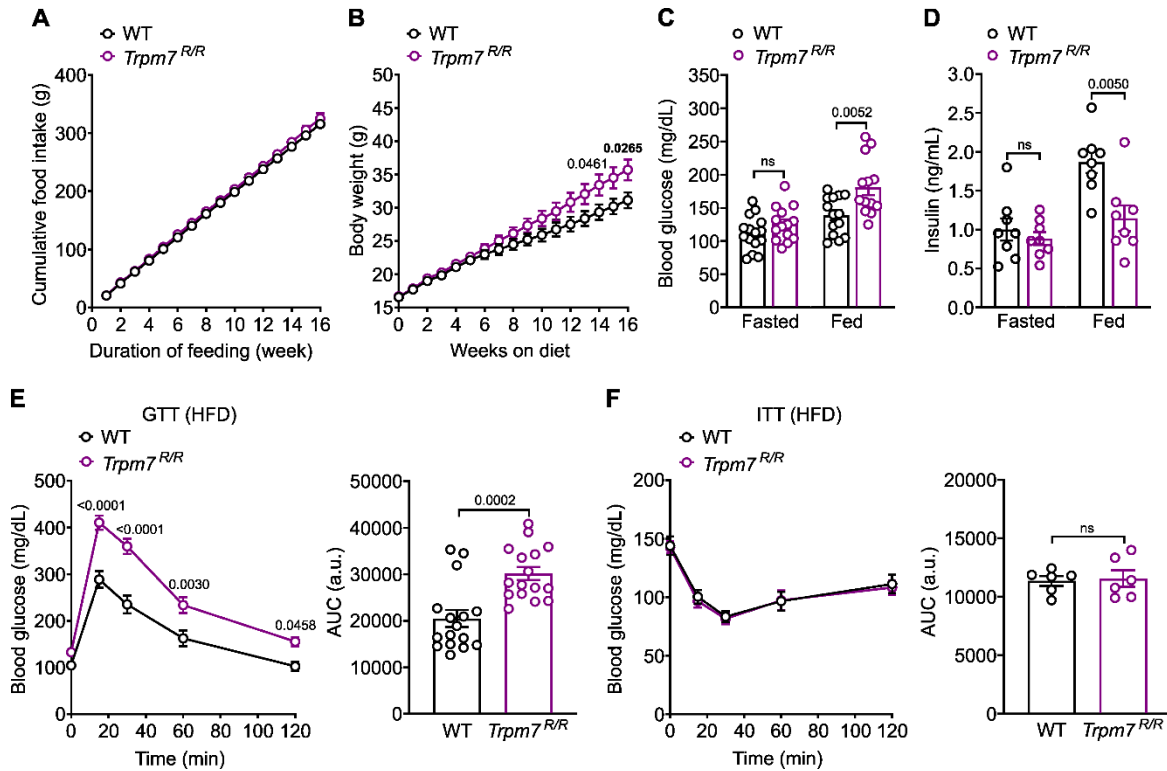
Figure 7 TRPM7 kinase disruption impairs glucose homeostasis in obese mice. Adult mice (*Trpm7^R/R* and control littermates) maintained on a HFD for 16-wks. (**A**) Cumulative food intake ($n \geq 6$ mice per genotype), (**B**) body weight ($n \geq 14$ mice per genotype), (**C**) blood glucose (mg/dL) in freely fed ($n \geq 14$ mice per genotype) or fasted ($n \geq 12$ mice per genotype) and (**D**) plasma insulin levels (ng/mL) in freely fed ($n = 8$ mice per genotype) or fasted (16 hours overnight) ($n = 8$ mice per genotype) in male and female *Trpm7^R/R* and control littermate mice were measured. (**E, F**) Blood glucose levels (mg/dL) before and within 2 hours after i.p. injection of (E) glucose (2 g/kg of body weight) and (F) insulin (0.75 U/kg of body weight) in WT and *Trpm7^R/R* mice (left panels) and area under the curves (AUC in mg/dL × min; right panels). For glucose tolerance test (GTT; E) mice were fasted overnight ($n \geq 20$ mice per genotype) and for insulin tolerance test (ITT; F) mice were fasted for 4 hours at the onset of the light cycle ($n \geq 14$ mice per genotype). Data show means ± S.E.M. and statistical differences were assessed by unpaired two-tailed Student's t-test (C, D, E right, F right) or two-way ANOVA (E, F, left panels). Circles in bar graphs represent single values. *P* values are shown above the bars. (ns, not significant)

964

965

966

967

968

969

970

971

972
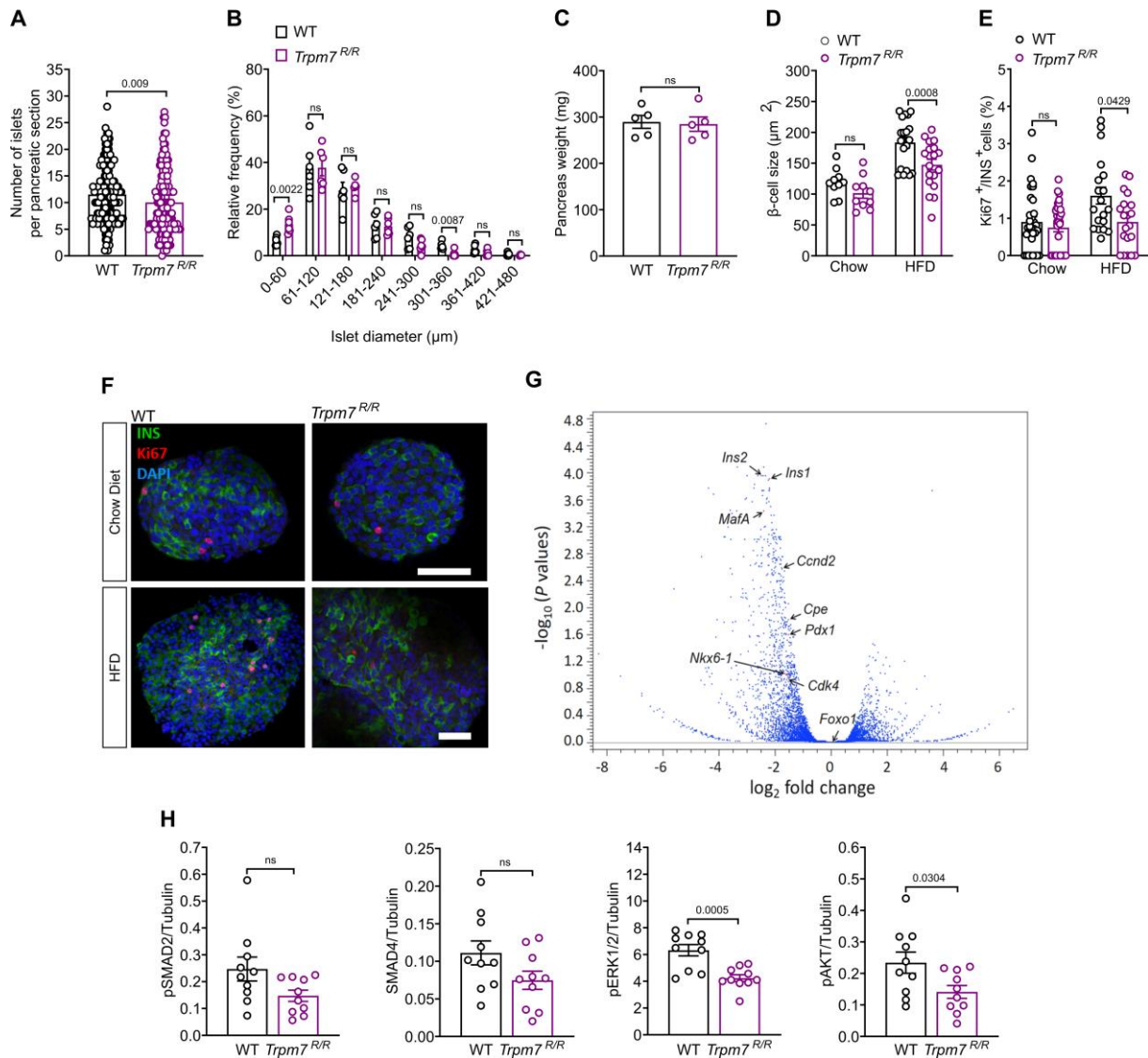
Figure 8 TRPM7 kinase disruption reduces compensatory β-cell responses due to a mitigated AKT/ERK signaling. (**A**) Number of islets per pancreatic cryosection (n = 144 slides, 3 mice per genotype), (**B**) relative frequency plot of islet diameter comparing WT with $Trpm7^{R/R}$ islets (n = 144 slides, 6 mice per genotype). (**C**) Pancreas weight of WT and $Trpm7^{R/R}$ mice maintained on a HFD for ~16-wks (n = 5 mice per genotype). (**D**) β-cell size (≥ 10 islets, at least 3 mice per genotype) and, (**E**) percentage of Ki67-positive cells from the population (100%) of the insulin-positive cells per pancreatic islet in WT and $Trpm7^{R/R}$ mice under the chow or HFD for 16-wks (n = 20, 5 mice per genotype). (**F**) Confocal images of WT and $Trpm7^{R/R}$ islets stained for DAPI (blue), insulin (green) and Ki67 (red). The scale bar represents 100 μm. (**G**) For RNA-seq analysis, islet RNA was collected from $Trpm7^{R/R}$ mice and the control littermates that had been maintained on a HFD for ~16-wks (n = 3 mice per genotype, age: ~24-wks). Volcano plot with downregulated and upregulated genes. Differentially expressed genes (DEGs) were identified (P<0.05) by using EdgeR method. DEGs are expressed as $\log_2$ fold change over control with an adjusted P value for each gene. (**H**) Assessment of the activity of the cell signaling molecules SMAD2, 4, ERK1/2, and AKT using multi-Plex assay and phospho-specific antibodies on lysates of isolated islets from WT and $Trpm7^{R/R}$ mice (n = 10, measured in duplicates, 10 mice per genotype) under 16-wks of HFD. Data are normalized to Tubulin content. Data show means ± S.E.M. and statistical differences were assessed by Mann-Whitney test (A) or unpaired two-tailed Student's t-test (B, C, D, E, H). Circles in bar graphs represent single values. P values are shown above the bars. (ns, not significant)